IRIS SEGMENTATION AND NORMALIZATION APPROACH

Mahboubeh Shamsi, Puteh Bt Saad, Abdolreza Rasouli
Faculty of Computer Science & Information System
University Technology Malaysia, Johor, Malaysia
mahboubehshamsi@yahoo.com, drputeh@gmail.com, rs.reza@gmail.com

Abstract: Iris is a desirable biometric representation of an individual for security-related applications. However the iris segmentation and normalization process is challenging due to the presence of eye lashes that occlude the iris, the dilation of pupils due to different light illumination and several other uncontrolled factors. In this work, we enhanced Daugman method to locate the iris and normalized it from polar to Cartesian coordinate. Iris is located by using a variable parameter binning approach. The algorithm is tested using iris images from CASIA database and MMU database. The percentage detection on MMU iris database is 99% and that of CASIA is 98%. Our approach is feasible to produce an iris template for identity identification and biometric watermarking application.

Keywords: iris recognition, biometric identification, recognition, normalization, automatic segmentation.

1. INTRODUCTION

A biometric system provides automatic recognition of an individual based on a unique feature possessed by an individual. Biometric systems have been developed based on fingerprints, facial features, voice, hand geometry, handwriting, the retina [1], and the one presented in this paper, the iris.

The first phase of iris Biometric systems is capturing the sample of the iris. Then iris samples are preprocessed and segmented to locate the iris. Once the iris is located, it is then normalized from polar coordinate to Cartesian. Finally a template representing a set of features from the iris is generated. The iris template can then be objectively compared with other templates in order to determine an individual's identity. Most biometric systems allow two modes of operation. An enrolment mode for adding templates to a database, and an identification mode, where a template is created for an individual and then a match is searched from a database of pre-enrolled templates.

Iris biometric has the following desirable properties, firstly an iris image is unique, the statistical probability that two irises would be exactly the same is estimated at 1 in 10^{72} [20].

Two different irises are extremely unlike to be equal, even in the case of genetically identical twins [2]. Secondly, the iris is stable and reliable since it does not vary with age and no foreign material can contaminate the iris, contact lens or spectacle do not hinder the capturing of the iris. Thirdly the iris fulfills the aliveness check (contraction of the pupil in response to light), where an imposter is unable to provide a fake iris image and finally it can be easily captured.

1.1. The Human Iris

The thin circular diaphragm, which separate between the cornea and the lens of the human eye is iris. The iris is perforated close to its centre by a circular aperture known as the pupil. The sphincter and the dilator muscles, which adjust the size of the pupil, can control the light entering through the pupil. The average diameter of the iris is 12 mm [2]. The iris consists of layers, the epithelium layer and the stroma layer. The epithelium layer contains dense pigmentation cells. The stroma layer that lies above the epithelium layer contains blood vessels, pigment cells and two iris muscles.

The color of the iris depend to density of stroma pigmentation determines. The surface of the multi-layered iris that is visible includes two sectors that are different in color [3], an outer ciliary part and an inner pupillary part. These two parts are divided by the collarette – which appears as a zigzag pattern. The iris is formatted of the third month of embryonic life [3]. In during the first year of life the unique pattern on the surface of the iris is formed. Formation of the unique patterns of the iris is random and not related to any genetic factors [4]. But the pigmentation of the iris is dependent on genetics. This is only and one character that depend on genetics. Also this character determines the color of it. Due to the epigenetic nature of iris patterns, the two eyes of an individual contain completely independent iris patterns, and identical twins possess uncorrelated iris patterns [3].

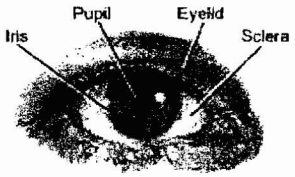

Figure 1. Human eye components

2. IRIS RECOGNITION

Figure 2 illustrated steps of recognize an iris from the eyes. In Iris Acquisition the eye image is captured. In Segmentation, the iris region in an eye image is located. A dimensionally consistent representation of the iris region is created in the normalization step.

Finally a template containing only the most discriminating features of the iris is generated in the feature encoding stage.

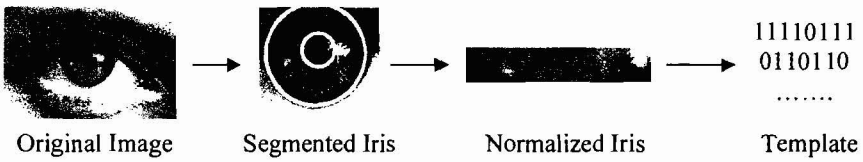

Figure 2. Iris Recognition Process

3. SEGMENTATION

In segmentation two circles are utilized to separate between iris/sclera boundary and iris/pupil boundary. The eyelids and eyelashes normally occlude the upper and lower parts of the iris region.

The success of a segmentation process depends on the imaging quality of eye images [7]. An individual with darkly pigmented irises display a low contrast between the pupil and iris region if the image is acquired under natural light, making segmentation more difficult [8]. An automatic segmentation algorithm based on the circular Hough transform is employed by Wildes et al. [5], Kong and Zhang [9], Tisse et al. [6], and Ma et al. [10]. These parameters are the centre coordinates x_c and y_c, and the radius r, which are able to define any circle according to the equation:

$$x_c^2 + y_c^2 - r^2 = 0 \tag{1}$$

Wildes et al. and Kong and Zhang also make use of the parabolic Hough transform to detect the eyelids, approximating the upper and lower eyelids with parabolic arcs, which are represented as;

$$\left(-(x-h_j)\sin\theta_j + (y-k_j)\cos\theta_j\right)^2 = a_j\left((x-h_j)\cos\theta_j + (y-k_j)\sin\theta_j\right) \tag{2}$$

Where

The controls the curvature is: a_j

The peak of the parabola is: (h_j, k_j)

The angle of rotation relative to the x-axis is: θ_j

Daugman makes use of differential operator for locating the circular iris and pupil regions, and also the arcs of the upper and lower eyelids. The differential operator is defined as

$$\max_{(r,x_p,y_o)}\left|G_\delta(r)*\frac{\partial}{\partial_r}\oint_{r,x_0,y_0}\frac{I(x,y)}{2\pi r}d_s\right| \qquad (3)$$

The eye image is: $I(x,y)$

The radius to search for is: r

The Gaussian smoothing function is: $G_\delta(r)$

And s is the contour of the circle given by r, x_0, y_0. The operator searches for the circular path where there is maximum change in pixel values, by varying the radius and centre x and y position of the circular contour.

Ritter et al. [17] make use of active contour models for localizing the pupil in eye images. Pre-set internal and external forces are responded with active contours .now active contours respond by deforming internally or moving across an image .this process continue until equilibrium is reached. The contour includes some vertex. These vertices have positions that are changed by two opposing forces:

- An internal force: It depends on the desired characteristics
- An external force: It depends on the image

Each vertex is moved between t and t+1 by

$$V_i(t+1)=V_i(t)+F_i(t)+G_i(t) \qquad (4)$$

- The internal force is: F_i
- The external force is: G_i
- The position of vertex i is: V_i

For localization of the pupil region we need two forces:

- The internal forces: they are calibrated so that the contour forms a globally expanding discrete circle.
- The external forces: they are usually found using the edge information.

In order to improve accuracy Ritter et al. use the variance image, rather than the edge image. 1D Gabor filters is useful for detecting Separable eyelashes, since the convolution of a separable eyelash with the Gaussian smoothing function results in a low output value. Another model is The Kong and Zhang model also makes use of connective criterion, so that each eyelash's point must connect to another eyelash's point or eyelid's point. Wildes et al suggested the vertical direction with Gradients for the outer iris/sclera boundary [4]. For the

inner iris/pupil boundary, Vertical and horizontal gradients were weighted equally. A modified version of Kovesi's Canny edge detection `MATLAB function [12] was implemented, which allowed for weighting of the gradients. In order to ensure the iris detection is efficient and accurate, boundary between iris and sclera circle is detected using Hough Transform in the iris region, instead of the whole eye region, since the pupil is always within the iris region.

3.2. Iris Localization

Base on Daugman operator, we proposed a slight nonlinear modification and reformulate the operator for speeding up the computation. The form is:

$$\max_{(n\Delta r, x_0, y_0)} \left| \sum_k \{ \frac{(G_\sigma(a_0) - G_\sigma(a_1)) \sum_m I(b_x, b_y)}{\Delta r \sum_m I(c_x, c_y)} \} \right| \tag{5}$$

With

$$a_0 = (n-k)\Delta r, a_1 = (n-k-1)\Delta r,$$
$$b_x = k\Delta r \cos(m\Delta\phi) + x_0,$$
$$b_y = k\Delta r \sin(m\Delta\phi) + y_0,$$
$$c_x = (k-2)\Delta r \cos(m\Delta\phi) + x_0,$$
$$c_y = (k-2)\Delta r \sin(m\Delta\phi) + y_0$$

For each (r, x_0, y_0) we must survey two sums over m that is in numerator and denominator and sum over k with one multiplication in numerator.

Based on Daugman method, we construct a kind of circular edge detector by using a series of binned images as illustrated in Figure 3.

This algorithm includes the set of potential center of pupil. But we assume that the actual center of image (center of pupil) is covered by the area of the dark pixel of the lowest resolution. But in higher resolution, this area covered by a number of pixels that is up to the relevant binning factor.

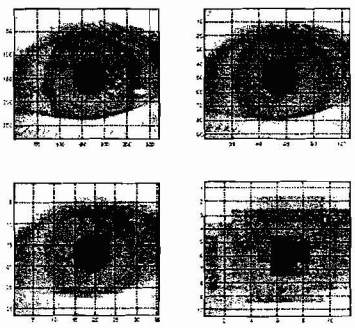

Figure 3. An example series of binned images

All of images are obtained from higher resolution by binning, except the input image $I^{(0)}$ so that $I^{(k)} = \mathrm{B}\{I^{(k-1)}, f\}$,where f is the factor of binning.

For circular edge detection we use this function:

$$\sum_{(x,y)\in C} \left\langle \nabla I(x,y), \vec{r} \right\rangle \tag{6}$$

that $\langle .,. \rangle$ is inner product, $\nabla I(x,y)$ is the gradient of input image I at the point of analysis (x, y), For rotating around the potential center (x_0, y_0) we use $\vec{r}$, For defining the coordinates of the point of analysis as

$$x = x_m = x_0 + [r\cos\alpha_m] \tag{7}$$

$$y = y_m = y_0 + [r\sin\alpha_m] \tag{8}$$

That

M And $\alpha_m = 2\pi m/M$ is the number of points taken in to integration over the circle. Also for integer value operator we use the value of 3.

For defining by simple differences in two orthogonal directions of the input image, we use ∇I that as follows:

$$\nabla I = (I_x, I_y) \tag{9}$$

$$I_x(x,y) = I(x+1,y) - I(x-1,y) \tag{10}$$

$$I_y(x,y) = I(x,y+1) - I(x,y-1) \tag{11}$$

The problem of 3 is that it's up to the length $r = |\vec{r}|$ so that it refers circles of larger radiuses. For solution of this problem, we use $\vec{v} = \vec{r}/r$ so $v = 1$ and version of 3 takes the form

$$\sum_{m=0}^{M-1} \left\langle \nabla I(x_m, y_m), \vec{v}_m \right\rangle \tag{12}$$

That

$$\vec{v}_m = (\cos\alpha_m, \sin\alpha_m)$$

Based on the above equations, as follows are the steps taken to implement the algorithm:

1. Get an input image I .
2. we use $I_k = \mathrm{B}\{I_{K-1}, f\}, k = 1..K$ for series of binned images
3. For I_K , find a minimum and after that assume it is a center $(x_0^{(K)}, y_0^{(K)})$ of the pupil.
4. For each image $I^{(K)}$ $k = 0..K$ starting from more to less binned images.
5. construct a set of potential center around the point defined by initial values obtained as the result of the previous stage

$$\left(x_0^{(K)}, y_0^{(K)}\right) \in C^{(K)} \tag{13}$$

Where

$$C^{(K)} = \left\{\left(\hat{x}_0^{(K)} - [f_k/2]\right)..\left(\hat{x}_0^{(K)} + [f_k/2]\right)\right\} \times \left\{\left(\hat{y}_0^{(K)} - [f_k/2]\right)..\left(\hat{y}_0^{(K)} + [f_k/2]\right)\right\} \tag{14}$$

6. construct a set of potential radiuses

$$r^{(K)} \in \left\{\left(\hat{r}^{(K)} - [f_k/2]\right)..\left(\hat{r}^{(K)} + [f_k/2]\right)\right\} \tag{15}$$

7. find

$$\left(\breve{r}, \breve{x}, \breve{y}\right) = \arg\max_{(r,x,y)} \sum_{m=1}^{M} \left(I_x(x_m, y_m)\cos\alpha_m + I_y(x_m, y_m)\sin\alpha_m\right) \tag{16}$$

8. recomputed $\left(\breve{r}^{(K)}, \breve{x}^{(K)}, \breve{y}^{(K)}\right)$ to the finer grid using f_K

$$\left(\breve{r}^{(K-1)}, \breve{x}^{(K-1)}, \breve{y}^{(K-1)}\right) = f_K\left(\breve{r}^{(K)}, \breve{x}^{(K)}, \breve{y}^{(K)}\right) \tag{17}$$

4. NORMALIZATION

In the normalization, iris region is transformed so that it has fixed dimensions to allow comparisons between same iris images. The inconsistencies between same eye images are due to stretches of the iris caused by dilation of pupil from different illumination. Among other factors that cause dilation are; eye rotation, camera rotation, head tilt and varying image distance. The good normalization process must produce different iris regions for different iris, in the same condition and it must produce constant dimensions for the same iris in different condition. Another great challenge is that the pupil region is not always concentric within the

iris region, and is usually slightly nasal [2]. Daugman's rubber sheet model explains remap of each iris region's point to the polar coordinates (r,θ)

The distance $[0,1]$is: r

The angle $[0,2\pi]$is: θ

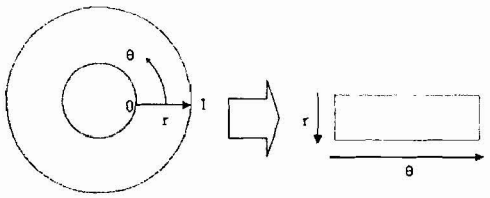

Figure 4. Daugman's rubber sheet model

The remapping of the iris region from (x,y) Cartesian coordinates to the normalized non-concentric polar representation is modeled as

$$I(x(r,\theta),y(r,\theta)) \rightarrow I(r,\theta) \tag{18}$$

With

$$\begin{aligned} x(r,\theta) &= (1-r)x_p(\theta)+rx_1(\theta) \\ y(r,\theta) &= (1-r)y_p(\theta)+ry_1(\theta) \end{aligned} \tag{19}$$

The iris region image is: $I(x,y)$

The original Cartesian coordinates are: (x,y)

The normalized polar coordinates are: (r,θ)

The coordinates of the pupil and iris boundaries along the θ direction are: x_p, y_p and x_1, y_1. The rubber sheet model is useful for accounting pupil dilation and size inconsistencies. This model however does not compensate for rotational inconsistencies.

For this problem, two iris templates are aligned with matching in shifting the iris templates in the θ direction.

4.1. Image Registration

The Wildes et al. system employs an image registration technique. This system for alignment, uses the geometrically warps of acquired image $I_a(x,y)$with a database include selected image $I_d(x,y)$ [4]. For closing the correspond points of new image with reference

image, we need the mapping function. The mapping function $(u(x,y),v(x,y))$ to transform the original coordinates is:

$$\int_x \int_y (I_d(x,y) - I_a(x-u, v-y))^2 d_x d_y \tag{20}$$

While being constrained to capture a similarity transformation of image coordinates (x,y) to (x',y'), that is

$$\begin{pmatrix} x' \\ y' \end{pmatrix} = \begin{pmatrix} x \\ y \end{pmatrix} - sR(\phi)\begin{pmatrix} x \\ y \end{pmatrix} \tag{21}$$

The scaling factor is: s

The matrix representing rotation by ϕ is: $R(\phi)$ [4].

4.2. Algorithm

Our algorithm on normalization of iris regions is based based on Daugman's rubber sheet model. Since the pupil can be non-concentric to the iris, a remapping formula is needed to rescale points depending on the angle around the circle. This is given by

$$r' = \sqrt{\alpha}\beta \pm \sqrt{\alpha\beta^2 - \alpha - r_I^2} \tag{22}$$

With

$$\alpha = o_x^2 + o_y^2$$
$$\beta = \cos\left(\pi - arcton\left(\frac{o_y}{o_x}\right) - \theta\right) \tag{23}$$

Where

The displacement of the centre of the pupil relative to the centre of the iris is given by o_y, o_x the distance between the edge of pupil and the edge of iris at an angle is: r'

Around the region is: θ

The radius of the iris is: r_I

In order to prevent non-iris region data from corrupting the normalized representation, data points which occur along the pupil border or the iris border are discarded same as Daugman's rubber sheet model.

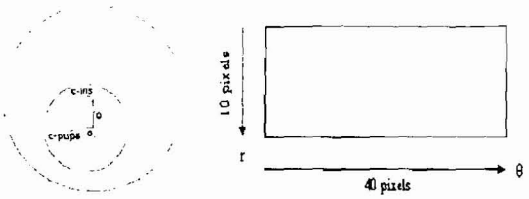

Figure 5. Outline of the normalization process with radial resolution of 10 pixels, and angular resolution of 40 pixels. Pupil displacement relative to the iris centre is exaggerated for illustration purposes.

5. RESULT

The above algorithm is implemented with Delphi programming language. It is tested using CASIA and MMU database [13]. In this case, more than 100 irises are randomly selected among of above databases. During detecting iris by this algorithm, most important thing is setting correct parameters. There are four parameters in the algorithm:

1. Smoothing Factor: This parameter is used in binning stage and indicates the width of binning square.
2. Binning Stage: It means that how many times the algorithm should binns the original image.
3. Suggest Radious: The radious of pupil in last binned stage.
4. Circle Sample: The number of points taken in to integration over the circle.

We have tested the algorithm in three different phases. In first phase all parameters are fixed for all images. We use Smoothing Factor = 3, Binning Stage = 4, Suggest Radius = 1 and Circle Sample = 64. The results are summarized in table.1.

TABLE I. EXECUTION RESULT WITH FIXED PARAMETERS

Iris Database	Percentage of Correctness		
	Correct Detect	*Correct Pupil or Correct Iris*	*Wrong Detect*
CASIA	73	16	11
MMU Iris Database	77	14	9

In this phase, we see that, wrong detections could be corrected by changing the parameters. For example, as you can see in Figure 6, the iris didn't detected correctly in left image, but by changing smoothing factor to 5, it has been reclaimed (see right image).

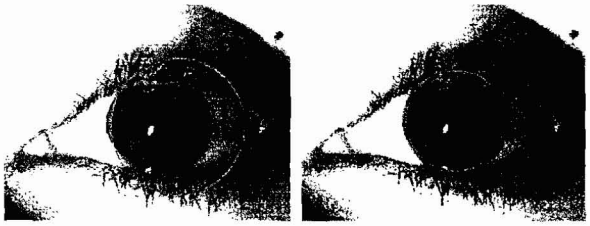

Figure 6. Left – Wrong Detection, Right – Reclaim by changing parameters.

In the second phase, we try to change parameters for wrong detections and test again to obtain a better result. By default we set the parameters similar as before, however in wrong detection we adjust the parameters until it is correctly detected. The results of second phase are shown in Table.II.

TABLE II. EXECUTION RESULT WITH NONFIXED PARAMETERS

Iris Database	Percentage of Correctness		
	Correct Detect	*Correct Pupil or Correct Iris*	*Wrong Detect*
CASIA	91	8	1
MMU Iris Database	94	5	1

It is observed that the results are significantly improved, but still there is some incorrect detection. In some cases, the pupil can be correctly detected, conversely incorrect detecting the pupil. After adjusting the value of the parameter, pupil is wrongly detected. In the third phase, different parameter values are adopted to improve the detection rate. The results of the third phase are summarized in Table.III. The final detection of some iris images is depicted in Fig 7.

TABLE III. EXECUTION RESULT WITH SEPARATE PARAMETERS

Iris Database	Percentage of Correctness	
	Detected	*Undetected*
CASIA	98	2
MMU Iris Database	99	1

Figure 7. Rightly Detected Iris a)MMU - b)CASIA

The normalisation process proved to be successful and some results are shown in Figure 8. However, the normalisation process is unable to perfectly reconstruct the same pattern from

images with varying amounts of pupil dilation, since deformation of the iris results in small changes of its surface patterns.

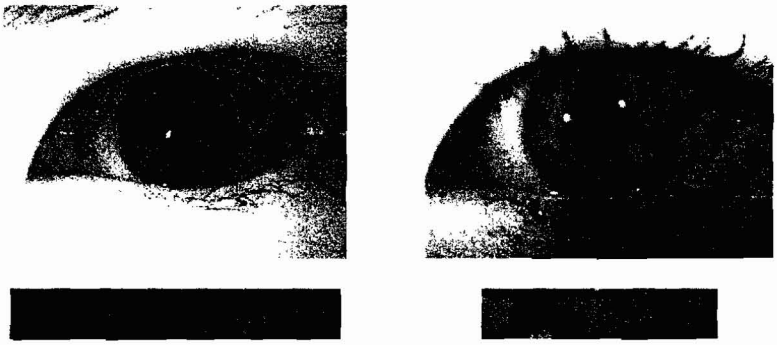

Figure 8. Illustration of the normalisation process for two images of the same iris taken under varying conditions.

Normalisation of two eye images of the same iris is shown in Figure 8. The pupil is smaller in the bottom image, however the normalisation process is able to rescale the iris region so that it has constant dimension. In this example, the rectangular representation is constructed from (360 * (Iris Radius – Pupil Radius)) data points in each iris region. Note that rotational inconsistencies have not been accounted for by the normalisation process, and the two normalised patterns are slightly misaligned in the horizontal (angular) direction. Rotational inconsistencies will be accounted for in the matching stage.

6. DISCUSSION AND CONCLUSION

As we have shown in the previous section, the critical step of the algorithm is setting the correct parameters. By using fixed parameters values, the algorithm automatically detects both the iris and the pupil. However, the rate of correct detection is low and it is not acceptable. Conversely by allowing manual intervention of parameters setting by the user for wrong detection, the accuracy rate increases as shown in Fig 9.

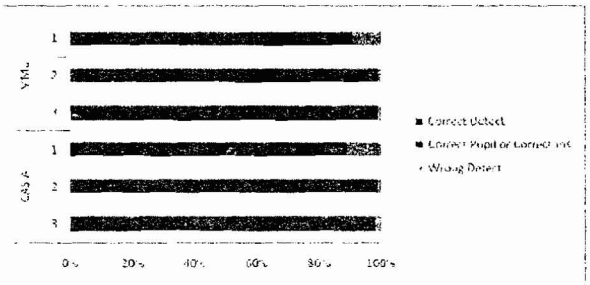

Figure 9. Percentage of Accuracy in Three Phases.

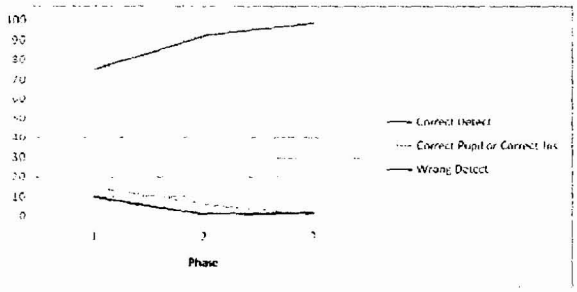

Figure 10. Final Success and Error Rate and Auto Detectability

As shown in Fig. 10, with a high quality images, auto detection produces encouraging results. On the other hand poor iris images need user-intervention to increase the rate of correct iris and pupil detection. The poor image quality is due to the presence of shadow especially in corners that contribute to the wrong detection of center point. Another potential problem is associated with luminosity in some images that hinder the detection process. Further problem is due to the irregular image dimension. To overcome the above problems, we can either use more than one images or incorporating an intelligent technique to automatically adjust the associated parameters for correct detection. Another challenging problem that we encounter during the normalization stage is the effect of eye lashes towards the iris. We do not have to perform the noise removal if both iris and eye lashes have similar colours. Noise here is indicated by the presence of eye lashes. However, we need to remove the noise from the iris, if iris and eye lashes have different colours. The noise will affect the accuracy of a template generated from a normalized iris in our next venture.

REFERENCES

[1] Sanderson S., Erbetta J. Authentication for secure environments based on iris scanning technology. IEE Colloquium on Visual Biometrics, 2000.

[2] Daugman J. How iris recognition works. Proceedings of 2002 International Conference on Image Processing, Vol. 1, 2002.

[3] Wolff E. Anatomy of the Eye and Orbit. 7th edition. Lewis H. K. & LTD Co., 1976.

[4] Wildes R. Iris recognition: an emerging biometric technology. Proceedings of the IEEE, Vol. 85, No. 9, 1997.

[5] Wildes R., Asmuth J., Green G., Hsu S., Kolczynski R., Matey J., McBride S. A system for automated iris recognition. Proceedings IEEE Workshop on Applications of Computer Vision, Sarasota, FL, pp. 121-128, 1994.

[6] Tisse C., Martin L., Torres L., Robert M. Person identification technique using human iris recognition. International Conference on Vision Interface, Canada, 2002.

[7] Chinese Academy of Sciences – Institute of Automation. Database of 756 Greyscale Eye Images. http://www.sinobiometrics.com Version 1.0, 2003.

[8] Barry C., Ritter N. Database of 120 Greyscale Eye Images. Lions Eye Institute, Perth Western Australia.

[9] Kong W., Zhang D. Accurate iris segmentation based on novel reflection and eyelash detection model. Proceedings of 2001 International Symposium on Intelligent Multimedia, Video and Speech Processing, Hong Kong, 2001.

[10] Ma L., Wang Y., Tan T. Iris recognition using circular symmetric filters. National Laboratory of Pattern Recognition, Institute of Automation, Chinese Academy of Sciences, 2002.

[11] Ritter N. Location of the pupil-iris border in slit-lamp images of the cornea. Proceedings of the International Conference on Image Analysis and Processing, 1999.

[12] Kovesi P. MATLAB Functions for Computer Vision and Image Analysis.Available at: http://www.cs.uwa.edu.au/~pk/Research/MatlabFns/index.html

[13] Daugman J G. Biometric personal identification system based on iris analysis [P].US Patent 5291560, 2004-03-01

[14] Oppenheim A., Lim J. The importance of phase in signals. Proceedings of the IEEE 69, 529-541, 1981.

[15] Field D. Relations between the statistics of natural images and the response properties of cortical cells. Journal of the Optical Society of America, 1987.

[16] http://www.cbsr.ia.ac.cn/IrisDatabase.htm

[17] http://www.oki.com/en/press/2006/z06114e.html

[18] http://www.iridiantech.com/products.php?page=4

[19] http://www.oki.com/jp/FSC/iris/en/m features.html

[20] Williams G. O, "Iris recognition technology," Iridian technologies, Tech.Rep., 2001